CrystEngComm

Accepted Manuscript

ROYAL SOCIETY OF CHEMISTRY

www.rsc.org/crystengcomm

Distribution of CSL grain boundaries in oriented cemented carbides

Xilong Wang, Xiaoyan Song*, Haibin Wang, Xuemei Liu, Xingwei Liu, Guangsheng Guo

College of Materials Science and Engineering, Key Laboratory of Advanced Functional Materials, Education Ministry of China, Beijing university of Technology, Beijing 100124, China

*E-mail: xysong@bjut.edu.cn

Abstract: The WC-Co cemented carbide bulk materials with anisotropic distribution of specific WC planes were prepared by spark plasma sintering (SPS) using different pre-sintering temperatures as 850^{o}C, 900^{o}C and 1000^{o}C at a constant pressure of 60 MPa. The coincident site lattice (CSL) grain boundaries were characterized and the anisotropic distribution of CSL boundaries was demonstrated. The combined effects of the composite powder and SPS parameters on the formation of the anisotropic CSL boundaries distribution were analyzed. The mechanisms were proposed that the CSL grain boundaries distribution can be tailored by adjusting the composition of the composite powder and SPS processing such as pre-sintering temperature, sintering pressure and its working stage. The findings facilitate to obtain a beneficial CSL grain boundaries distribution that enhances mechanical properties in certain directions of the cemented carbide.

Keywords: cemented carbide; orientation texture; CSL grain boundary; anisotropic distribution; sparking plasma sintering

1 Introduction

WC-Co cemented carbides are important engineering materials widely used in mining, machining, cutting, drilling and wear-resistant parts due to their good combined performance of hardness and toughness [1, 2]. In the microstructure, the interface (including grain boundaries and phase boundaries) characteristics play a

critical role in the mechanical properties of the cemented carbide [3-7]. Particularly, the coincident site lattice (CSL) grain boundaries, which have fairly low energy, have attracted increasing attention of researchers due to their special effect on improvement of the material properties [8]. As reported in the literature, the CSL grain boundaries in the WC-Co cemented carbides are mainly Σ13, which can be described as rotation of 27.796^{o} around the [0001] axis (abbreviated as 27.796^{o}/[0001]), and Σ2, which is considered as a 90^{o} rotation of two prismatic planes along the [10-10] direction [9-12].

The amount and distribution of CSL grain boundaries in the cemented carbides are influenced by many factors such as WC grain size [9], Co volume fraction and distribution on the WC matrix [13, 14]. In the previous work, the CSL grain boundaries were generally studied in the isotropic cemented carbides. The distribution characteristics, as well as the influencing factors, of the CSL grain boundaries in the cemented carbides with oriented WC grains have been rarely investigated so far. Moreover, how to increase the fraction of the low energy CSL grain boundaries in the cemented carbides and correlate with the mechanical properties are still big challenges in the questions of cemented carbides preparation.

In this work, the WC-12wt. %Co cemented carbides with highly orientated WC grains and distinctly different fraction and distribution characteristics of CSL grain boundaries were fabricated. The microstructure textures were characterized and the formation mechanisms were analyzed. The results of the present study facilitate the design and preparation of the cemented carbides with tailored amount of CSL grain boundaries, which is favorable to enhance the orientational mechanical properties.

2 Experimental

The tungsten oxide ($WO_{2.9}$), cobalt oxide (Co_3O_4) and carbon black powders were used as raw materials. The raw powders were mixed by high energy ball milling, and the as-milled powder mixture was put in a vacuum furnace for the in situ reduction and carbonization reactions to synthesize the WC-Co composite powder [15].

Subsequently, the composite powder was consolidated by spark plasma sintering (SPS) [16, 17]. Two sets of SPS parameters were used, one group parameters are heating to and pre-sintering at 900^{o}C for 30min then sintering at 1250^{o}C for 10min; another group parameters are heating to and pre-sintering at 1000^{o}C for 30min then sintering at 1250^{o}C for 10min. The constituent phases of the sintered bulk materials were examined by X-ray diffraction (XRD) with Cu K_{α} radiation. The orientation analysis of the microstructures was performed by the electron back scattering diffraction (EBSD) using a high speed Hikiari camera incorporated in the field emission environmental scanning electron microscope. Based on the EBSD technique, the grain boundary characteristics distribution was studied in a reliable statistical volume range [18].

3 Results

3.1 Distribution characteristics of specific grain boundaries

The phase constitutions on the cross-sections vertical (VD) and parallel (PD) to the sintering pressure direction of the prepared bulk material are shown in Fig. 1(a-d), respectively. From the comparison of the XRD results, it can be seen that on the VD cross-section the relative density of the basal plane (0001) with respect to the prism planes of (10-10) and (10-11) in the 1000^{o}C pre-sintered bulk sample is smaller than that in the 900^{o}C pre-sintered bulk sample. To quantify the fraction of certain WC planes, the XRD patterns were integrated to calculate the areas of WC planes to estimate the corresponding area fraction of the plane. The area fractions of WC planes on the VD and PD cross-sections are shown in Fig. 1(e) and (f), respectively. On the VD cross-section of the 900^{o}C and 1000^{o}C pre-sintered samples, the area fractions of the (0001) basal planes are 31.7% and 21.1%, respectively. However, on the PD cross-section of the 900^{o}C and 1000^{o}C pre-sintered samples, the area fractions of the (0001) basal planes are 40.8% and 29.5%, respectively. The values indicate clearly that the distribution of the basal plane is anisotropic in different directions. Moreover, even in the same orientation, the distribution of the basal plane depends strongly on the processing of the material preparation.

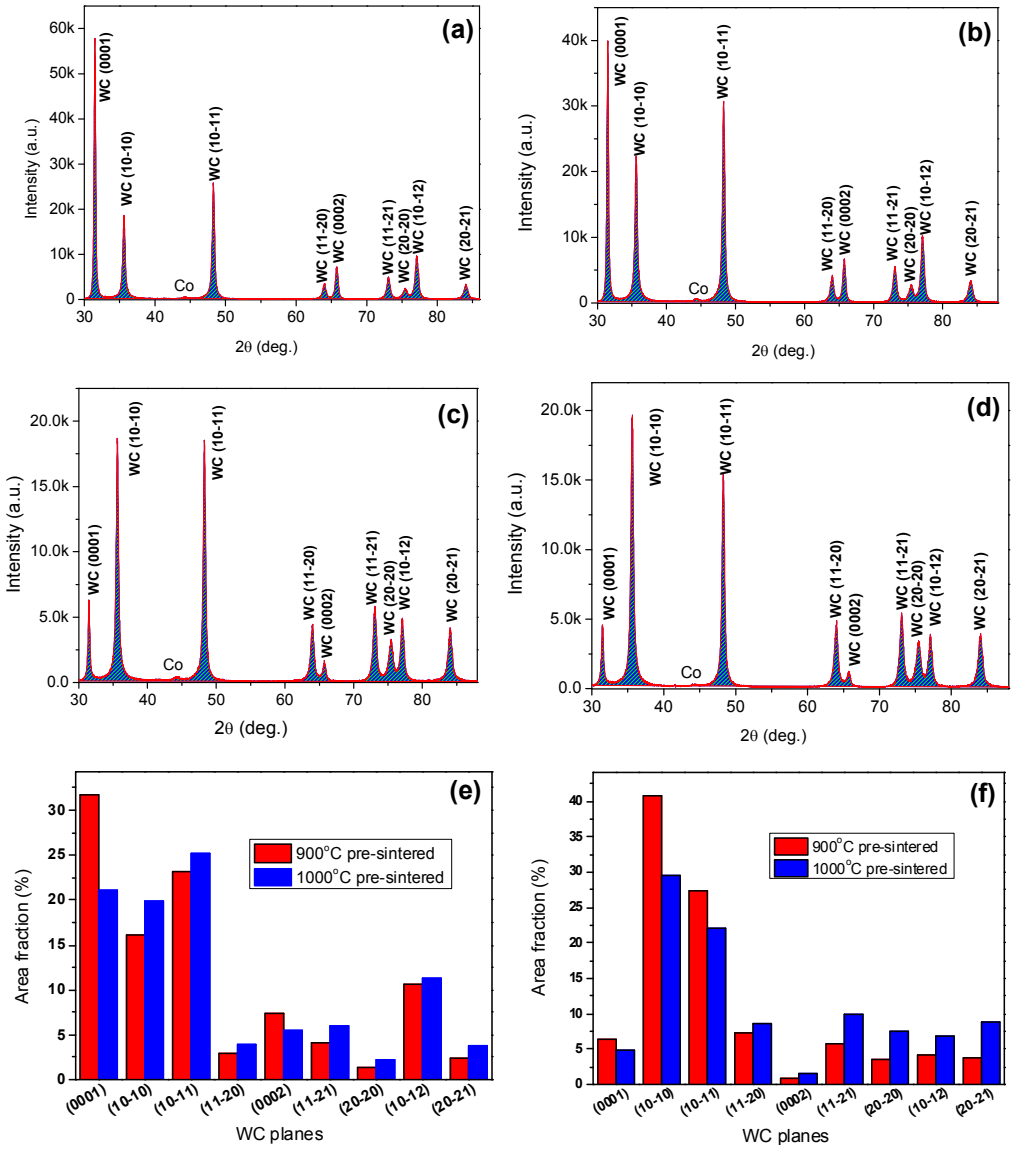

Fig. 1 XRD patterns and WC plane area fractions on different cross-sections of the prepared bulk sample: (a) XRD patterns on the VD cross-section of the 900°C pre-sintered sample; (b) XRD patterns on the VD cross-section of the 1000°C pre-sintered sample; (c) XRD patterns on the PD cross-section of the 900°C pre-sintered sample; (d) XRD patterns on the PD cross-section of the 1000°C pre-sintered sample; (e) area fractions of WC planes on VD cross-section; (f) area fractions of WC planes on PD cross-section.

The microstructures on the VD and PD cross-sections of the prepared bulk

material are shown by IPF maps in Fig. 2(a), (b), (e) and (f), respectively. In a IPF map, the color of a grain specifies its orientation according to the color distribution as indicated in the orientation legend, thus the carbide grains are observed with preferred crystallographic orientations. On the VD cross-section, the grains with red color and colors close to red are dominant, and the grains are mainly equiaxed, as shown in Fig. 2(a) and (b). The orientation texture degree of the WC grains in the 900°C and 1000°C pre-sintered samples are characterized by the inverse pole figures (IPF), as shown in Fig. 2(c) and (d), with the unit of the contours in multiples of random distribution (MRD). Both the IPF charts exhibit strong {0001} orientation texture of the WC grains. From the comparison of Fig. 2(c) and (d), the {0001} orientation texture in the 900°C pre-sintered sample is obviously stronger (with an increase of about 31%) than that in the 1000°C pre-sintered sample.

Fig. 2(e) and (f) show the IPF maps on the PD cross-section of the two kinds of bulk samples, with the characterization of the orientation texture of the WC grains shown in Fig. 2(g) and (h). It is observed that the orientation texture of the prism planes is stronger in the 900°C pre-sintered sample than that in the 1000°C pre-sintered sample, but the difference (with an increase of about 10%) is not as large as that on the VD cross-section of the two kinds of samples.

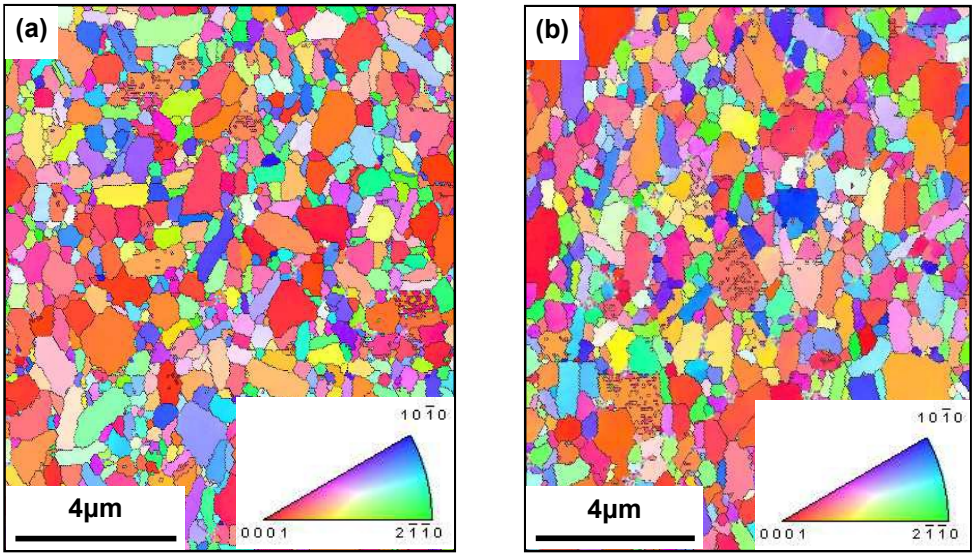

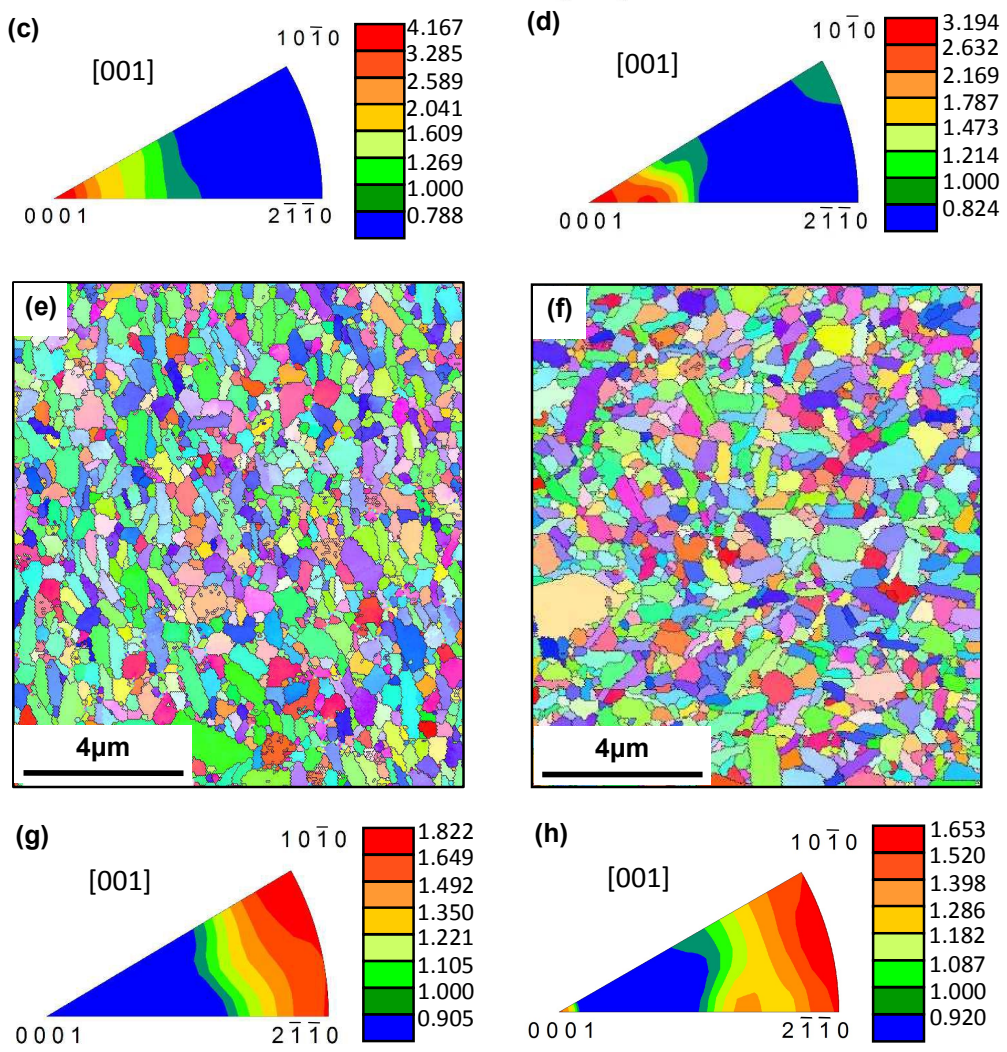

Fig. 2 Inverse pole figure maps on the VD and PD cross-sections of different samples with grain orientations determined by the orientation legend: (a), (c) on VD cross-section of the 900°C pre-sintered sample; (b), (d) on VD cross-section of the 1000°C pre-sintered sample; (e), (g) on PD cross-section of the 900°C pre-sintered sample; (f), (h) on PD cross-section of the 1000°C pre-sintered sample.

To examine the orientation texture of the Σ13 boundary planes, the grain boundary plane orientation distribution function (GBP-ODF) is studied by characterizing the grain boundary plane orientation with specific misorientation with

respect to 27.796° / [0001]. The results are illustrated in a stereographic projection, as shown in Fig. 3, with the unit of the contours in MRD, where a larger MRD value indicates a relatively higher frequency of the corresponding boundary plane orientation. For the two kinds of samples, the peak in the distribution of the Σ13 boundary plane orientations locates at the [0001] axis (as denoted by the hexagon in Fig. 3), this means that the Σ13 boundary plane is perpendicular to the common rotation axis. Therefore, the Σ13 boundary consists of the twisting (0001) planes in the neighboring grains. At the same time, the absence of a peak in the circle perpendicular to the [0001] axis implies that the Σ13 boundary seldom has an asymmetric tilt configuration. As compared in Fig. 3, in the 900°C pre-sintered sample, the distribution density of the Σ13 boundary plane on the VD cross-section has a maximum of 3.2 MRD while a maximum of 10.26 MRD on the PD cross-section. In the 1000°C pre-sintered sample, the distribution density of the Σ13 boundary plane has a maximum of 4.80 MRD on the VD cross-section and a maximum of 7.96 MRD on the PD cross-section. Both samples have a higher fraction of the Σ13 grain boundaries on the PD cross-section than that on the VD cross-section. Moreover, the anisotropy of the distribution of the Σ13 grain boundaries is much stronger in the 900°C pre-sintered sample than that in the 1000°C pre-sintered sample. The results indicate that the distinctly anisotropic distributions of the WC grain boundary orientations and the boundary plane characteristics are formed in the cemented carbide bulk materials when prepared with suitable processing parameters, even with the same initial composition.

From comparison of Figs. 3(a) and 3(c), it can be seen that the oriented distribution of Σ13 variants is stronger in the 1000°C pre-sintered sample than that of the 900°C pre-sintered sample. In the condition of increasing temperature at a constant axial pressure, WC grain growth occurs accompanied with grain rotation, which results in the decrease in the number of grain boundaries that are close to parallel to [0001]. Therefore, the fraction of Σ13 variants parallel to (0001) plane is increased from the 900°C to 1000°C pre-sintered sample.

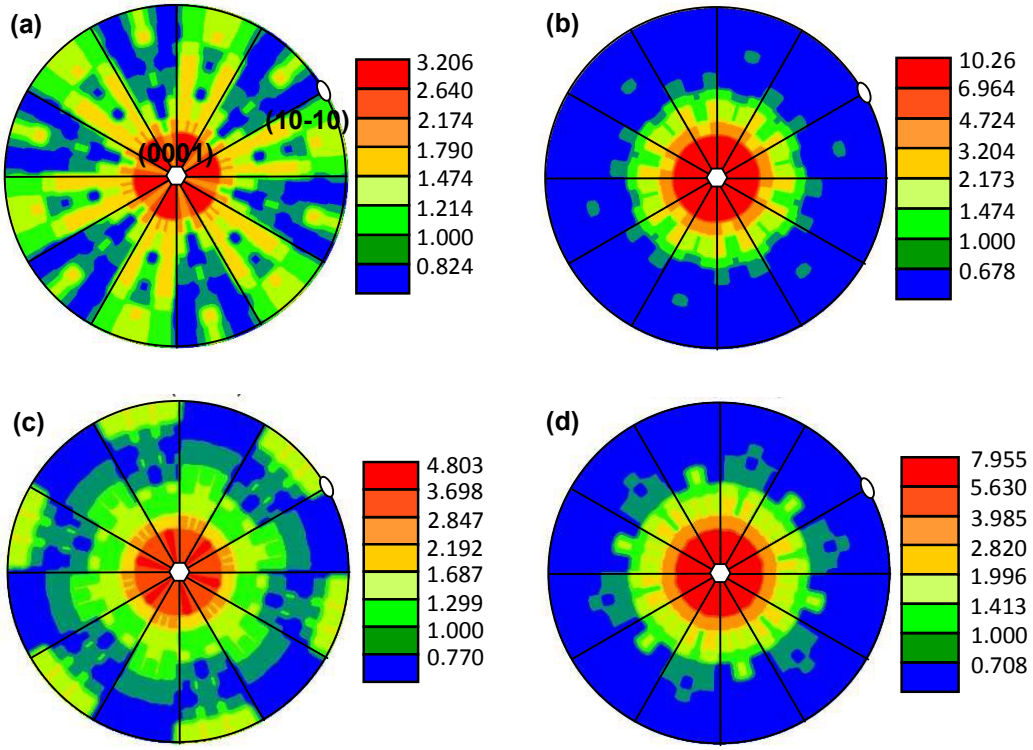

Fig. 3 Distribution of the Σ13 grain boundary plane orientations in the 900°C and 1000°C pre-sintered samples: (a) VD cross-section of the 900°C pre-sintered sample; (b) PD cross-section of the 900°C pre-sintered sample; (c) VD cross-section of the 1000°C pre-sintered sample; (d) PD cross-section of the 1000°C pre-sintered sample. The symbols of hexagon and oval denote the relative distribution density of the Σ13 boundary plane on the (0001) and (10-10) planes, respectively.

The GBP-ODF of the Σ2 boundary planes is obtained by characterizing the grain boundary plane orientations at a specific misorientation of 90^{o} / [10-10], as the results shown in Fig. 4. For both the VD and PD cross-sections, the largest distribution density of the Σ2 boundary plane orientations is at the axis [10-10], as indicated by the oval. This means that the probability that the Σ2 boundary plane distributes on the (10-10) plane is much higher than on other planes. Therefore, the Σ2 grain boundary consists of the twisting (10-10) planes in the neighboring grains. On the other hand, the Σ2 boundary can hardly have a tilt configuration that consists of a (0001) basal

plane in one grain against a (10-10) prismatic plane in the neighboring grain. It can be seen that in the 900°C pre-sintered sample, the relative distribution densities of the Σ2 twist boundaries are 52.7 MRD on the VD cross-section while 39.5 MRD on the PD cross-section. The result indicates that the Σ2 grain boundary has a clearly higher probability to distribute on the VD cross-section than on the PD cross-section. This tendency is even stronger in the 1000°C pre-sintered sample, with a relative distribution density of Σ2 boundaries as 58.7 MRD on the VD cross-section while 38.7 MRD on the PD cross-section. As compared with Fig. 3, it is obvious that the distribution of the Σ13 grain boundaries has a stronger anisotropy in the 900°C pre-sintered sample than in the 1000°C pre-sintered sample. However, the anisotropy of the distribution of the Σ2 grain boundaries is obviously stronger in the 1000°C pre-sintered sample. The measurements show that the distribution anisotropy of the specific Σ13 and Σ2 grain boundaries can be obtained in the cemented carbides, and the degree of the distribution anisotropy can be tailored by the processing.

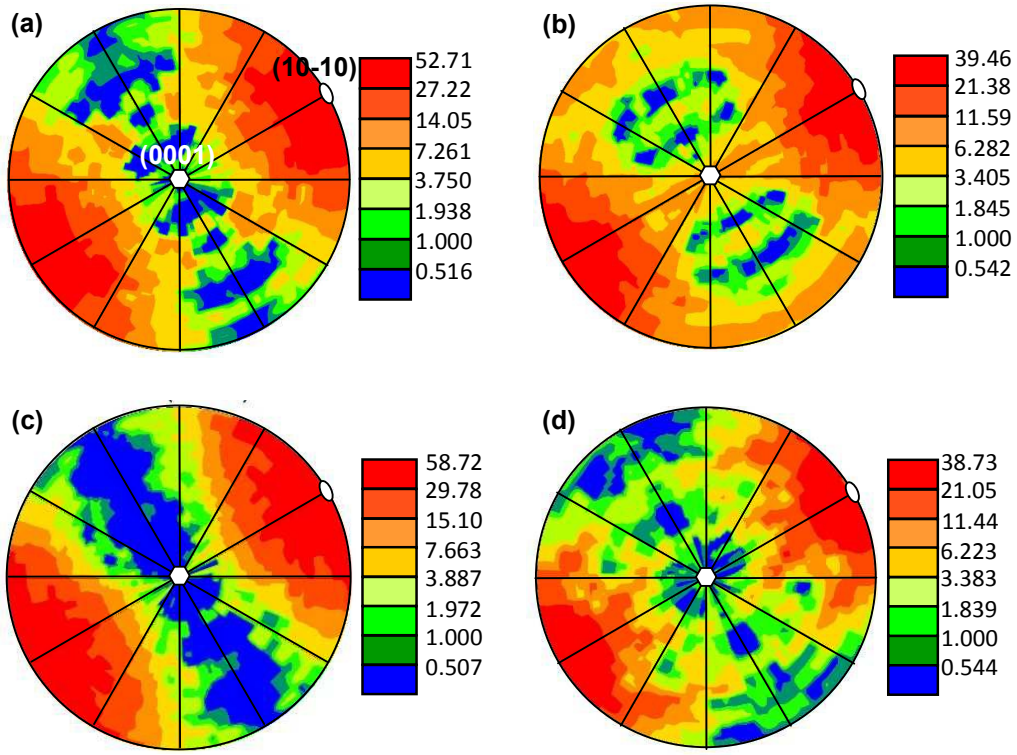

Fig. 4 Distribution of the Σ2 grain boundary plane orientations in the 900°C and 1000°C pre-sintered samples: (a) VD cross-section of the 900°C pre-sintered sample;

(b) PD cross-section of the 900°C pre-sintered sample; (c) VD cross-section of the 1000°C pre-sintered sample; (d) PD cross-section of the 1000°C pre-sintered sample. The symbols of hexagon and oval denote the relative distribution density of the Σ2 boundary plane on the (0001) and (10-10) planes, respectively.

To analyze the orientation relationship between the WC grains, the misorientation angle distributions are calculated and illustrated in Fig. 5. It can be seen that there are two peaks at 30° and 90° implying an obvious preference of the misorientation angle distribution. In spite of the difference in the frequency values, the two samples have a similar tendency: the frequency that the WC grain boundary misorientation has a angle of 30° is higher on the PD cross-section than that on the VD cross-section, in contrast, the misorientation angle as 90° has a higher frequency on the VD cross-section than on the PD cross-section. The finding confirms the results in Fig. 3 and Fig. 4, that the fraction of the Σ13 boundaries on the VD cross-section is obviously higher than that on the PD cross-section, while the tendency is inverse for the Σ2 boundaries.

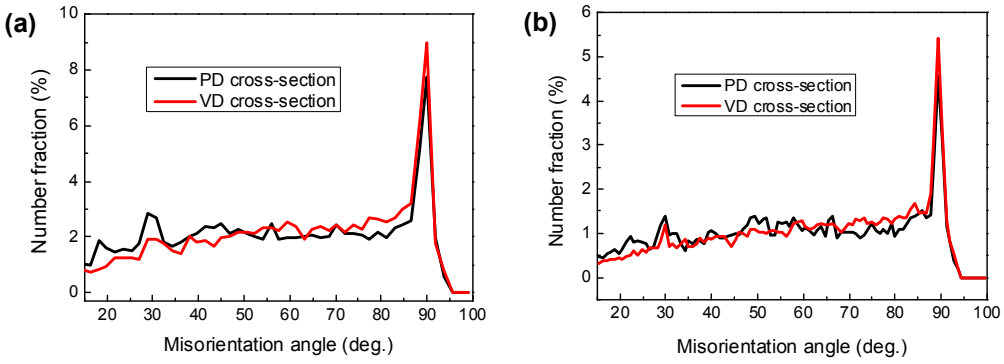

Fig. 5 Distribution of the grain boundary misorientation angles on the VD and PD cross-sections: (a) 900°C pre-sintered sample; (b) 1000°C pre-sintered sample.

3.2 Mechanism for anisotropy of specific grain boundaries distribution

It is known that the increase in the fraction of the CSL grain boundaries is

favorable for the mechanical properties in certain directions of the engineering materials [19]. However, the effective way to achieve a desirable CSL grain boundaries distribution is still an open question. Especially for the cemented carbides, though the influences of the grain size [5, 9], carbide volume fraction [5, 13], plastic deformation [20], densification method [21], and grain geometry and energy state [22-26] on the specific grain boundaries were studied, the consistent conclusions have not been recognized yet.

In the present work, a feasible approach is proposed by combined optimization of the composite powder and SPS sintering. When the composite powder contains a certain amount of carbon lack phases (η) such as Co_3W_3C (space group Fd3m [27]) and W_2C (space group P-312/m [28]), after fast consolidation by means of SPS with high sintering pressure, the oriented grain structure with relatively higher fraction of plate-like WC grains will be formed in the final WC-Co bulk material. The reason can be analyzed based on Figs. 6-8, which show the phase constitutions in the composite powders synthesized at 850, 900 and 1000°C, respectively, together with the diffraction of WC planes in the consolidated bulk samples. During the SPS process, the η phase existing in the composite powder reacts with the free carbon in the powder mixture, leading to the formation of new WC grains which grow on the basis of the flat η phase. During the rapid solid-state sintering densification, where the dissolution of WC in Co does not occur, the newly formed WC grains continue growing on the η phase, leading to the formation of the plate-like WC grains with its basal plane vertical to the sintering pressure.

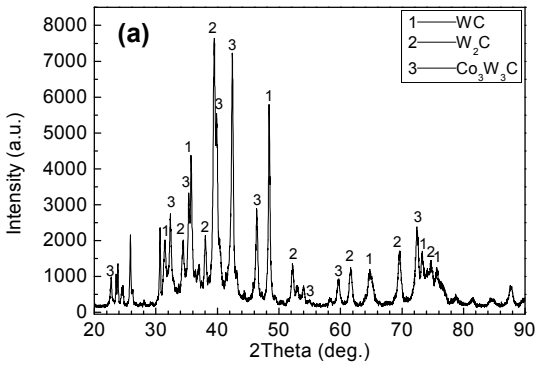

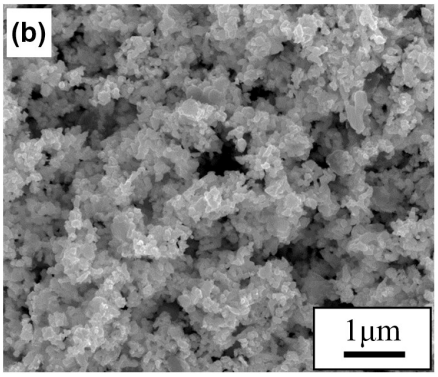

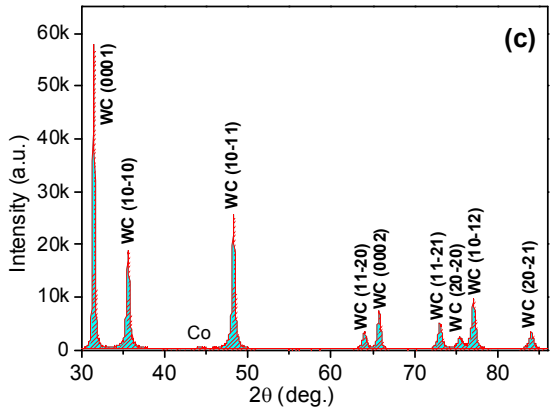

Fig. 6 Phase constitution (a) and SEM image (b) of the composite powder synthesized at 850^0C and the diffraction intensity of WC planes on VD cross-section of the sintered bulk material (c), where the fraction of η phase is the largest in the powder.

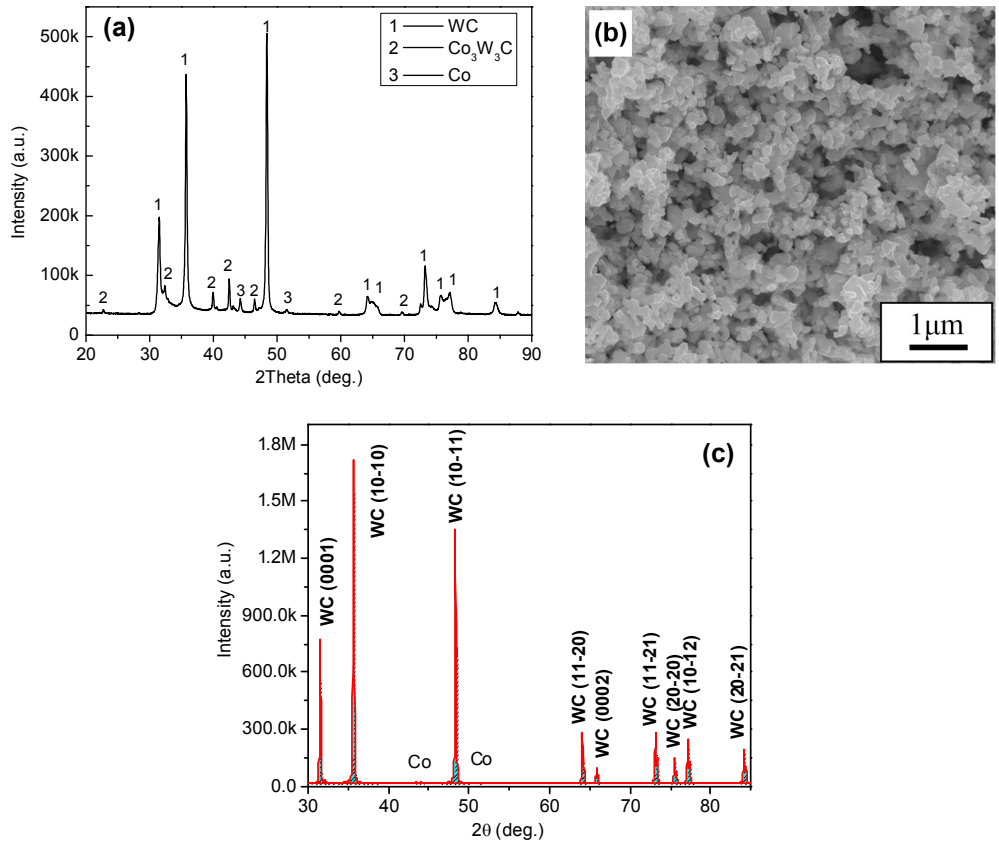

Fig. 7 Phase constitution (a) and SEM image (b) of the composite powder synthesized at 900^0C and the diffraction intensity of WC planes on VD cross-section of the sintered bulk material (c), where the fraction of η phase is the second largest in the powder.

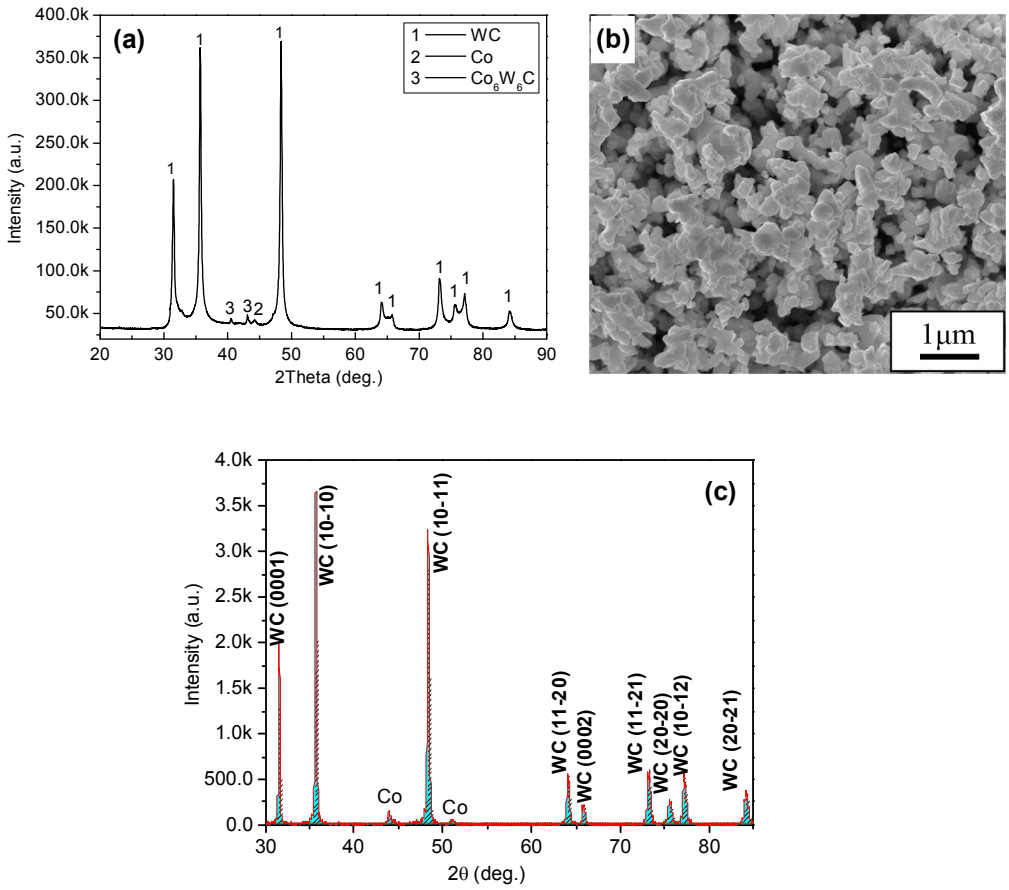

Fig. 8 Phase constitution (a) and SEM image (b) of the composite powder synthesized at 1000^{0}C and the diffraction intensity of WC planes on VD cross-section of the sintered bulk material (c), where the fraction of η phase is the smallest in the powder.

The fraction of the WC basal planes on the VD cross-section of the sintered bulk material is dominated by the amount of the η phase that transforms into the oriented WC during SPS sintering. Thus, the pre-sintering temperature affects the amount of newly formed oriented WC grains. As shown in Fig. 9, different pre-sintering temperature causes different relative diffraction intensities of the WC planes. In the range of the pre-sintering temperature from 850^{o}C to 1000^{o}C, the fraction of the WC basal planes on the VD cross-section reaches a maximum at the pre-sintering temperature of 900^{o}C. At 850^{o}C, the reaction between the η phase and carbon is insufficient, and the amount of the resultant plate-like WC grains is limited. While at 1000^{o}C the reaction is sufficient, and the number of WC nuclei is large, which results

in the impinging of new WC grains after a short time of growing. As a consequence, the equiaxed grains are formed instead of plate-like grains with prior orientation. At an intermediate temperature of 900°C, the nucleation and growth of WC grains are coordinated, with a moderate nucleation rate and subsequently a sufficient degree of grain growth, the well developed plate-like WC grains are formed in the sintered bulk material. According to the above mechanisms, under the condition of a constant amount of the η phase in the composite powder, the distribution of specific WC planes depends on the pre-sintering temperature. Since the anisotropic distribution of WC planes results in the anisotropy of the grain boundaries distribution, the distribution of the CSL grain boundaries can be optimized by the processing parameters.

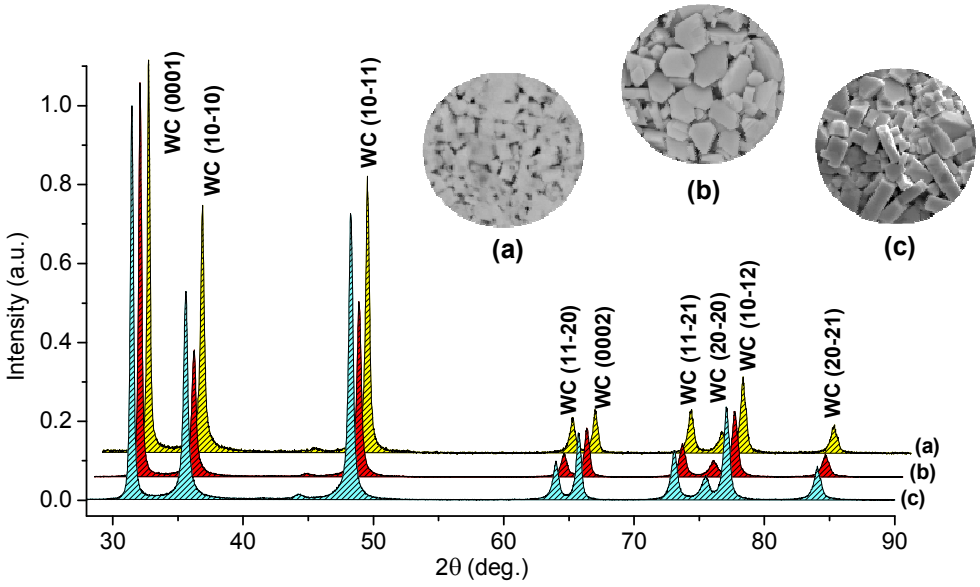

Fig. 9 Diffractions of WC planes on the VD cross-section of samples pre-sintered at different temperatures: (a) 850°C; (b) 900°C; (c) 1000°C. The insets are the corresponding microstructures.

Based on the finding that the oriented WC grains newly formed during SPS sintering are dominated by the reaction between the η phase and free carbon existing in the composite powder, one can be guided to design the microstructure with a beneficial CSL grain boundaries distribution. The important factors include the

composition of the composite powder, the pre-sintering temperature, and matching of the sintering pressure and its working stage. In the present experiments that other factors are fixed, the pre-sintering temperature of the composite powder is dominant for the distribution of the CSL grain boundaries. The results facilitate the development of cemented carbide materials and engineering products with enhanced properties in certain directions for service.

4. Conclusion

The cemented carbide bulk material with highly oriented plate-like WC grains was prepared by optimizing the pre-sintering temperature of SPS process for reaction between the η phase and free carbon existing in the WC-Co composite powder. It was found that the specific WC planes have anisotropic distribution, which leads to the anisotropy of the CSL grain boundaries distribution, i.e. the Σ13 grain boundaries have higher fraction on the PD cross-section than on the VD cross-section, while the Σ2 grain boundaries have higher fraction on the VD cross-section than on the PD cross-section. Guided by the disclosed mechanisms, one can tailor the distribution of the CSL grain boundaries by adjusting the composition of the composite powder and the SPS processing, e.g. pre-sintering temperature, external pressure and its working stage. The present results may assist the development of cemented carbide materials and engineering products with enhanced properties in certain directions by controlling the anisotropy of CSL grain boundaries distribution.

Acknowledgements

This work was supported by the National High-tech R&D Program of China (2013AA032001), the National Science Fund for Distinguished Young Scholars (51425101), the National Natural Science Foundation of China (51174009) and the Beijing Key Program of Natural Science Foundation (2131001).

References

[1] A. petersson, J. Ågren, Constitutive behaviour of WC–Co materials with different grain size sintered under load, *Acta. Mater,* 2004, 52, 1847-1858

[2] L. Fu, L. H. Cao, Y. S. Fan, Two-step synthesis of nanostructured tungstencarbide-cobalt powders, *Scripta. Mater*., 2001, 44, 1061-1068

[3] C. S. Kim, G. S. Rohrer, Geometric and crystallographic characterization of WC surfaces and grain boundaries in WC-Co composites, *Interface Sci*., 2004, 12, 19-27

[4] Y. Gao, X. Y. Song, H. B. Wang, X. L. Wang, X. M. Liu, Effect of carbon content on matching of key crystal planes in nanocrystalline cemented carbide, *CrystEngComm*., 2014, 16, 4935-4939

[5] C. S. Kim, T. R. Massa, G. S. Rohrer, Interface character distributions in WC-Cocomposites, *J. Am. Ceram. Soc*., 2008, 91, 996-1001

[6] X. Y. Song, Y. Gao, X. M. Liu, C. B. Wei, H. B. Wang, W. W. Xu, Effect of interfacial characteristics on toughness of nanocrystalline cemented carbides, *Acta. Mater*., 2013, 61, 2154-2162

[7] C. B. Wei, X. Y. Song, J. Fu, X. M. Liu, H. B. Wang, Y. Gao, Y. Wang, Simultaneously high fracture toughness and transverse rupture strength in ultrafine cemented carbide, *CrystEngComm*., 2013, 15, 3305-3307

[8] T. Watanabe, Grain boundary engineering: historical perspective and future prospects, *J. mater. Sci*., 2011, 46, 4095-4115

[9] X. K. Yuan, Grain boundary character distributions of coincidence site lattice boundaries in WC-Co composites with different WC grain sizes, *J. Alloy. Compd*., 2013, 579, 622-627

[10] S. Hagege, G. Nouet, and P. Delavignette, Grain boundary analysis in TEM, *Phys. Stat. Sol*., 1980, 61, 97-107

[11] J. Vicens, M. Benjdir, G. Nouet, A. Dubon, J. Y. Laval, Cobalt Intergranular Segregation in WC–Co Composites, *J. Mater. Sci*., 1994, 29, 987-94

[12] J. D. Kim, S. J. L. Kang, J. W. Lee, Formation of Grain Boundaries in Liquid‐Phase‐Sintered WC-Co Alloys, *J. Am. Ceram. Soc*., 2005, 88, 500-503

[13] C. S. Kim, T. R. Massa, G. S. Rohrer, Interface character distributions in WC-Co

composites, *Ceram. Int*., 2014, 40, 1873-1878

[14] C. S. Kim, T. R. Massa, G. S. Rohrer, Interface character distributions in WC-Co composites, *J. Am. Ceram. Soc*., 2008, 91, 996-1001

[15] W. B. Liu, X. Y. Song, J. X. Zhang, G. Z. Zhang, X. M. Liu, Preparation of ultrafine WC-Co composite powder by in situ reduction and carbonization reactions, *Int. Journal of Refractory Metals & Hard Materials*., 2009, 27, 115-120

[16] P. Puneet, R. Podila, S. Zhu, M. J. Skove, T. M. Tritt, J. He, A. M. Rao, Enhancement of Thermoelectric Performance of Ball-Milled Bismuth Due to Spark-Plasma-Sintering-Induced Interface Modifications, *Adv. Mater*., 2013, 25, 1033-1037

[17] Y. Dong, G. S. Nolas, Rapid crystal growth of type-II clathrates A8Na16Si136 (A=K, Rb, Cs) by spark plasma sintering, *CrystEngComm*., 2015, 17, 2242-2244

[18] W. Wisniewski, R. D. Kloe, C. Rüssel, EBSD-measurements of textured apatite glass-ceramics, *CrystEngComm*., 2015, 17, 2969-2973

[19] T. Watanabe, Grain boundary engineering: historical perspective and future prospects, *J. Mater. Sci*., 2011, 46, 4095-4115.

[20] X. K. Yuan, G. S. Rohrer, X. Y. Song, C. Harry, J. Li, Modeling the interface area aspect ratio of carbide grains in WC–Co composites, *Int. Journal of Refractory Metals & Hard Materials*., 2014, 44, 7-11.

[21] X. K. Yuan, X. Y. Song, H. Chien, J. Li, G. S. Rohrer, Effect of densification mechanism on the Σ2 grain boundary plane distribution in WC–Co composites, *Mater. Lett*., 2013, 92, 86-89

[22] S. Lay, M. Loubradou, Characteristics and Origin of Clusters in Submicron WC-Co Cermets, *Phil. Mag*, 2003, 83, 2669-79

[23] C. S. Kim and G. S. Rohrer, Geometric and Crystallographic Characterization of WC Surfaces and Grain Boundaries in WC-Co Composites, *Interface. Sci*., 2004, 12, 19-27

[24] M. Christensen ,G. WahnstrÖm, Effects of Cobalt Intergranular Segregation on Interface Energetics in WC-Co, *Acta Mater*., 2004, 52, 2199-2207

[25] J. D. Kim, S. J. Kang, and J.W. Lee, Formation of Grain Boundaries in Liquid Phase Sintered WC-Co Alloys, *J. Am. Ceram. Soc*., 2005, 88, 500-503

[26] V. Kumar, Z. Z. Fang, S. I. Wright, M. M. Nowell, An Analysis of Grain Boundaries and Grain Growth in Cemented Tungsten Carbide using Orientation Imaging Microscopy, *Metall. Mater. Trans. A*., 2006, 37, 599-607

[27] D. V. Suetin, I. R. Shein, A. L. Ivanovskii, Structural, electronic and magnetic properties of ŋ-carbides (Fe_3W_3C, Fe_6W_6C, Co_3W_3C and Co_6W_6C) from first principles calculations, *Physica. B*., 2009, 404, 3544-3549

[28] A. A. Sivkov, E. P. Naiden, A. Ya. Pak, Dynamic synthesis of ultradispersed crystalline phases of the C-N system, *J. Superhard Mater*., 2009, 31, 300-305

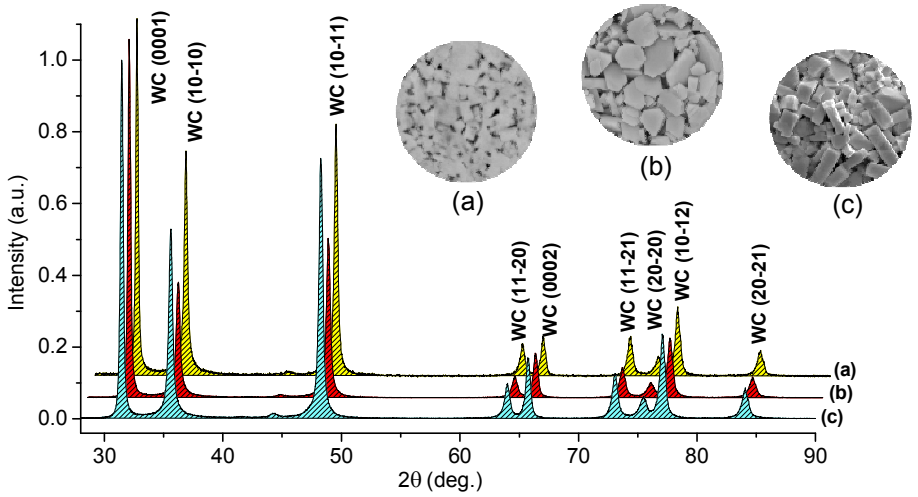

The anisotropy of distributions of specific WC planes and coincidence site lattice (CSL) grain boundaries can be tailored by adjusting the composition of WC-Co composite powder and its sintering parameters.